Naphthochromenones: Organic Bimodal Photocatalysts Engaging in Both Oxidative and Reductive Quenching Processes

RESEARCH ARTICLE

# Naphthochromenones as New Organic Photoredox Catalysts. Synthesis, Structure-Property Relationship and Applications

Javier Mateos,[a] Francesco Rigodanza,[a] Alberto Vega-Peñaloza,[a] Andrea Sartorel,[a] Mirco Natali, [b] Tommaso Bortolato,[a] Giorgio Pelosi,[c] Xavier Companyó,[a] Marcella Bonchio,[a] and Luca Dell'Amico*[a]

In memory of Dieter Enders (1964–2019) for his invaluable contribution to organic chemistry

**Abstract:** A novel class of naphthochromenone organic photocatalysts (PCs) with a peculiar absorption across the UV- and visible-light regions is reported. These PCs are synthesized in a straightforward manner starting from readily available materials. The synthesis allows the gram scale production of 12 different PCs with *ad hoc* photoredox properties, representing a new affordable option towards photoredox catalysis. Their distinctive photochemical and redox properties are assessed by absorption/emission spectroscopies and cyclic voltammetry, delineating robust structure-properties relationships, further supported by time-dependent density functional theory (TD-DFT) calculations. Remarkably, naphthochromenone PCs show an extremely wide redox window up to 3.35 V, accessible with simple illumination sources (>400 nm), maintaining all the advantages of simplicity and product stability of visible-light photocatalysis. Their strong excited state redox potentials, $PC^*/PC^{\bullet -}$ = up to 1.74 V and $PC^{\bullet +}/PC^*$ up to -1.83 V vs SCE, ensure the ability of performing both challenging oxidative and reductive photoredox processes. This class of PCs represents a new powerful tool in photocatalysis.

## Introduction

Solar light is an unlimited source of clean and renewable energy on Earth.[1] Its conversion into diverse energy forms is at the forefront of intense research in diverse scientific areas from biology to engineering. The chemical community, playing a central role across disciplines, has devoted enormous efforts in the development of novel and more efficient photocatalytic species, possibly capable of performing light-driven transformations in catalytic routines.[2] The utilization of these molecules has a direct impact on our every-day life – from the synthesis of polymers[3] to the more recent applications towards natural products synthesis or drug development.[4] Across the sun-light emission spectrum spanning from UV- to visible-light, it is possible to count on a variety of suitable PCs.[5] The research devoted to the identification of novel PCs[6] which can absorb low energy photons, even moving towards red light,[7] is extremely active.

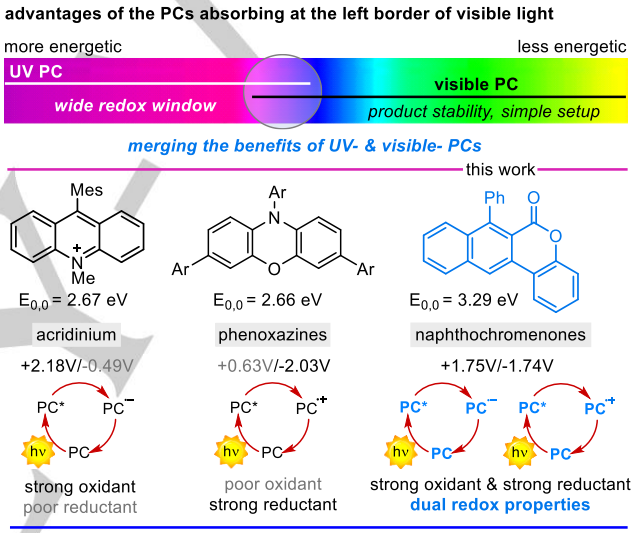


**Figure 1.** UV- and visible-light photocatalysis – main advantages (top) and selected examples of organic photoredox catalysts (PCs) absorbing in the cross-border region (bottom). Mes = mesityl. Ar = 2-naphtyl. Reported redox potentials vs SCE.

Conversely, the research of novel PCs which can absorb more energetic photons, has received less interest, although this research can open the way to new classes of PCs which combines the benefits of UV- and visible-light absorption. PCs which absorb UV-light (< 365 nm) usually generate highly energetic excited states,[5d,e] capable of performing extremely challenging photoreactions, where strongly oxidant or strongly reductant excited states are required. Their broad utilisation is hampered by: (i) the use of photons not abundant in the solar emission spectrum; (ii) the possible reagents or products decomposition, promoted by high-energy UV photons;[2a] and (iii) the need of specific irradiation sources (e.g. Hg- or Xe- lamps), and inert setups (e.g. quartz reaction vessels). On the other hand, visible-light absorbing PCs (> 400 nm), including metal-based PCs (e.g. Ru, Ir or Cu complexes)[5a-d] and organic dyes (e.g. rhodamines or eosin Y)[5e-g] generate less energetic excited states with respect to UV-PCs, but they can be efficiently used with less energetic and readily available light sources (e.g. compact fluorescence lamp = CFL or LED) and simple glass setups, with none or minor problems of product decomposition[2, 5a,b] while

[a] J. Mateos, F. Rigodanza, A. Vega-Peñaloza, A. Sartorel, T. Bortolato, X. Companyó, M. Bonchio, L. Dell'Amico
Department of Chemical Sciences
University of Padova Institution
Via Marzolo 1, 35131 Padova, Italy
E-mail: luca.dellamico@unipd.it
[b] M. Natali
Department of Chemical and Pharmaceutical Sciences
University of Ferrara Institution
Via Luigi Borsari 46, 44121 Ferrara, Italy
[c] G. Pelosi
Department of Chemistry, Life Sciences and Environmental Sustainability
Parco Area delle Scienze 17, 43124 Parma, Italy

Supporting information for this article is given via a link at the end of the document.

guaranteeing safer user operations. In general terms, a powerful PC combines the advantages of visible-light absorption with a redox window as wider as possible, efficiently catalysing the highest number of light-driven transformations. The combination of these features within a single molecular entity is a formidable challenge. A promising approach is based on the identification and use of a PC which absorbs at the border between UV- and visible-light (Figure 1, top). Theoretically, the absorption under this region (390-410 nm) will consent to access highly energetic excited states (typically > 2 eV), while using simple and safe setups and light sources, with definite advantages with respect to the accessible operational redox window. As a support of this assumption, acridinium and phenoxazine PCs,[5e] which mainly rely on the absorption in this border region, are characterized by wide redox windows (2.67 and 2.66 V for acridinium and phenoxazine, respectively, Figure 1). Consequently, they can generate highly oxidant (up to +2.18 V vs SCE for acridinium) or highly reductant (up to -2.03 V vs SCE for phenoxazine) excited states while using simple visible light sources.[5e] Recent reports have shown that structural modifications can fine-tune their potentials towards more balanced redox properties for exploiting them in both reductive and oxidative quenching cycles.[8a-c] Also cyanoarenes, another useful class of organic PCs, have been recently modified to address diverse synthetic challenges.[8e-h] Although this is often an effective strategy, it is not always possible to count on rational designed structure-property relationships. Additionally, complex structural modifications are not generally applicable to diverse class of PCs.[5-8] Thus, the identification and development of new PCs characterised by highly energetic excited states and powerful oxidative and reductive power accessible at >400 nm can open the way to unprecedented reactivity patterns.

We herein outline the identification of *6H*-naphthochromen-6-one (NTC) as an novel family of organic PCs (Figure 1, right). NTCs present an absorption spectrum at the border of visible-light, which guarantees the access of high energy excited state (up to 3.35 eV) with the use of simple visible light sources, maintaining both strong oxidative and reductive properties, E (PC*/PC$^{\bullet-}$) up to -1.83 V and E (PC$^{\bullet+}$/PC*) up to 1.74 V vs SCE. The identification of a scalable synthetic plan together with easy structural functionalisation lead to the generation of 12 diverse PCs at gram scale. Structure-photoredox property relationships are assessed in terms of HOMO-LUMO energy levels, absorption and emission, ground/excited state redox potentials, fluorescence quantum yield and excited state lifetime. Remarkably, the potential of this new class of PCs is demonstrated by the ability of catalysing a variety of transformations classically promoted by both UV- or visible-light absorbing PCs.

## Results and Discussion

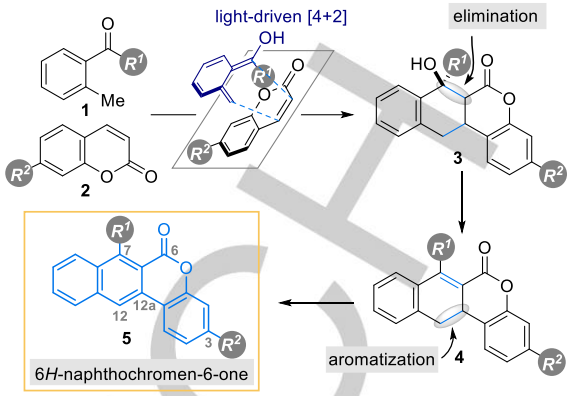


**Scheme 1.** Synthesis of PCs **5a-f** from carbonyl compounds **1a-c** and coumarins **2a-c**.

The identification of the NTC scaffold **5** as potential organic PC was stimulated by our previous works on the synthesis of the tetracyclic scaffolds **3**.[9] (Scheme 1).

**Table 1.** Synthesis of PCs **5a-f** from carbonyl compounds **1a-c** and coumarins **2a-c**.

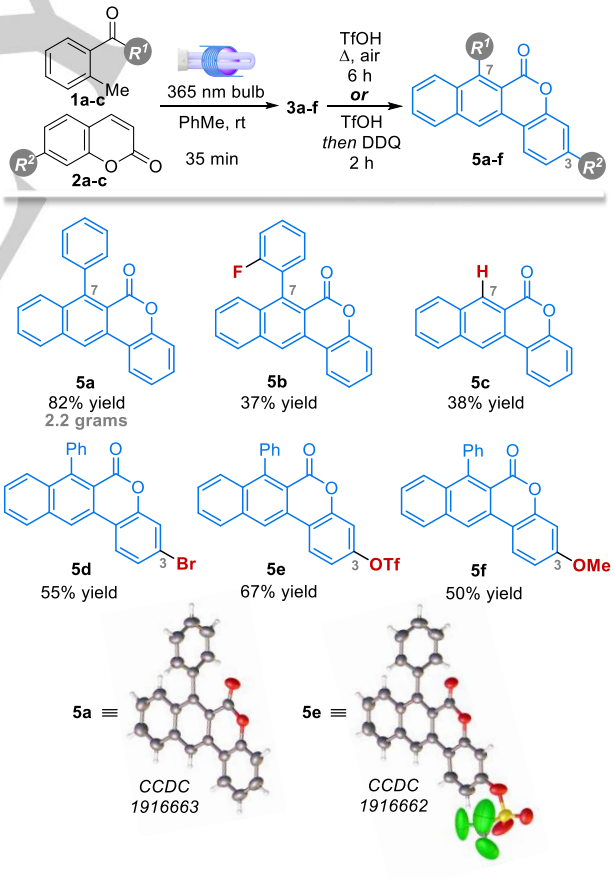

We envisaged compound **3**, derived from the reaction between the photoenol, generated upon light excitation of the corresponding benzophenones **1**,[10] and coumarins **2**, as precursor of NTC **5** through an elimination/aromatization sequence (Scheme 1).

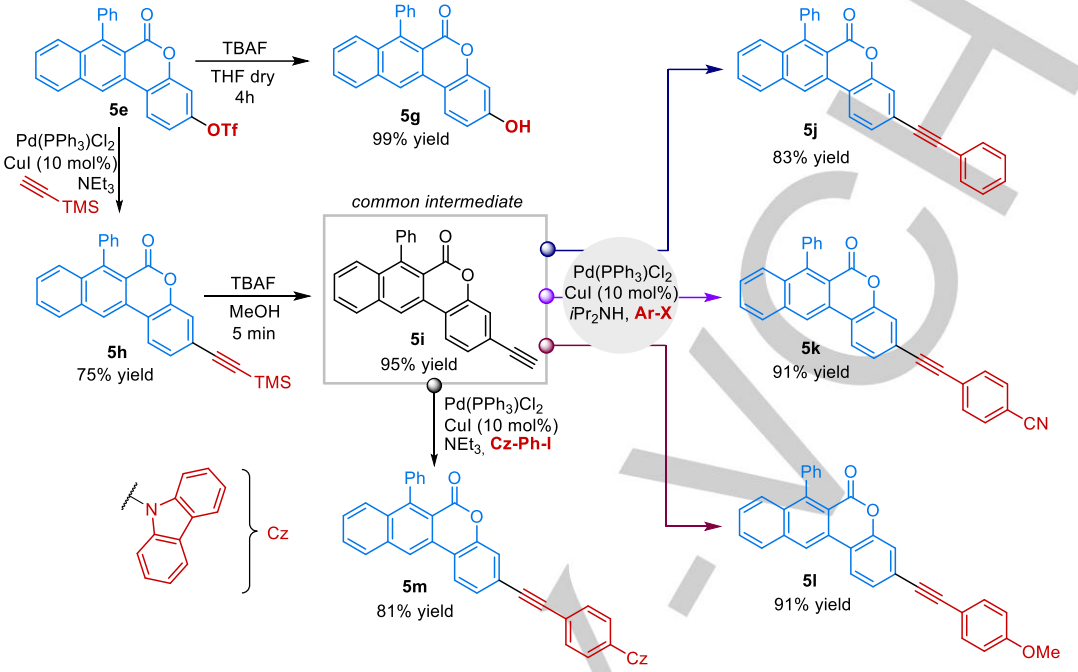


**Scheme 2.** Post-functionalization of PC **5e** for the synthesis of PCs **5g**,**h** and **5j**-**m**. All the yields refer to isolated yields. TBAF = tetrabutylammonium fluoride. Cz = carbazole. For **5j**-**5l** X = I, for **5k** X = Br.

We have to consider that both starting materials benzophenone **1** and coumarin **2** have distinctive absorptions under the UV region.[11] This fact also suggested a possible absorption at longer wavelengths of the more conjugated scaffold **5**. Once identified a general synthetic strategy (Scheme 1), suitable reaction conditions were developed and applied to diverse readily available starting materials **1a**-**c** and **2a**-**c**, allowing the easy tuning of the NTC scaffold at positions 3 and 7 (Table 1). We started the synthesis of differently substituted NTCs **5**, with the goal of defining structure-property relationships while generating a library of PCs with varied photoredox properties. The initial light-driven [4+2]-cycloaddition reaction between benzophenone **1a** and coumarin **2a** was performed under microfluidic conditions.[9b] Tetracyclic product **3a** formed rapidly within 35 min residence time. Isolation of **3a** and subsequent treatment with triflic acid (TfOH) delivered directly NTC scaffold **5a** without the need of any additional synthetic operation.[12] A simple recrystallization furnished compounds **5a**-**5c** with variations at position 7 in moderate to high overall yields 37%-82%. Compounds **5d**-**5f**, bearing diverse groups at position 3 were synthesized in overall yields spanning from 36% to 67%. In these cases, a two-step elimination-aromatization sequence resulted in improved yields and diminished reaction time (See SI). Remarkably, the developed synthetic protocol was scaled-up without any yield drop, producing up to 2.2 g of **5a**. The structure of **5a** and **5e** were confirmed by X-ray analysis on single crystal. Prompted by the simple synthetic route which allows the fast and effective synthesis of diverse scaffolds **5**, we explored the impact of diverse structural post-functionalization. We identified **5e**, bearing an OTf group at position 3, as a versatile precursor to diverse PCs scaffolds. The hydroxyl functionality was easily deprotected by treatment with tetrabutylammonium fluoride (TBAF) solution, delivering PC **5g** in quantitative yield (Scheme 2 top, left). Next, scaffold **5h** was synthetized (95% yield) in order to evaluate the effect of an increased conjugation. Interestingly, despite being an intermediate for the assembly of other PCs, **5h** showed promising photoredox properties (*vide infra*). After a simple desilylation step, **5i** was obtained in high yield after simple filtration on a silica-pad (Scheme 2, grey box). At this juncture, diverse aromatic substituents bearing electron withdrawing or electron donating groups were introduced by a simple synthetic operation (Scheme 2, right and bottom). PCs **5j**-**5m** were synthesized in excellent yields spanning from 81% to 91% by using **5i** and selected aryl halides through a Sonogashira cross-coupling. With a wide library of novel organic PCs in hand, we next examined their photoredox properties.

**Analysis of the Photochemical and Redox Properties.** We first looked at the properties of PCs **5** in both the excited and ground states, crucial in effecting the photocatalytic performances. **5a** showed a distinctive absorption spectrum with a peak centred at 380 nm ($\varepsilon$ = 5100 $M^{-1}cm^{-1}$) and a shoulder at 360 nm, tailing up to 440 nm (Figure 2a, black line), and three distinct peaks between 300-330 nm ($\lambda 1$ = 299, $\lambda 2$ = 313 and $\lambda 3$ = 327 nm).

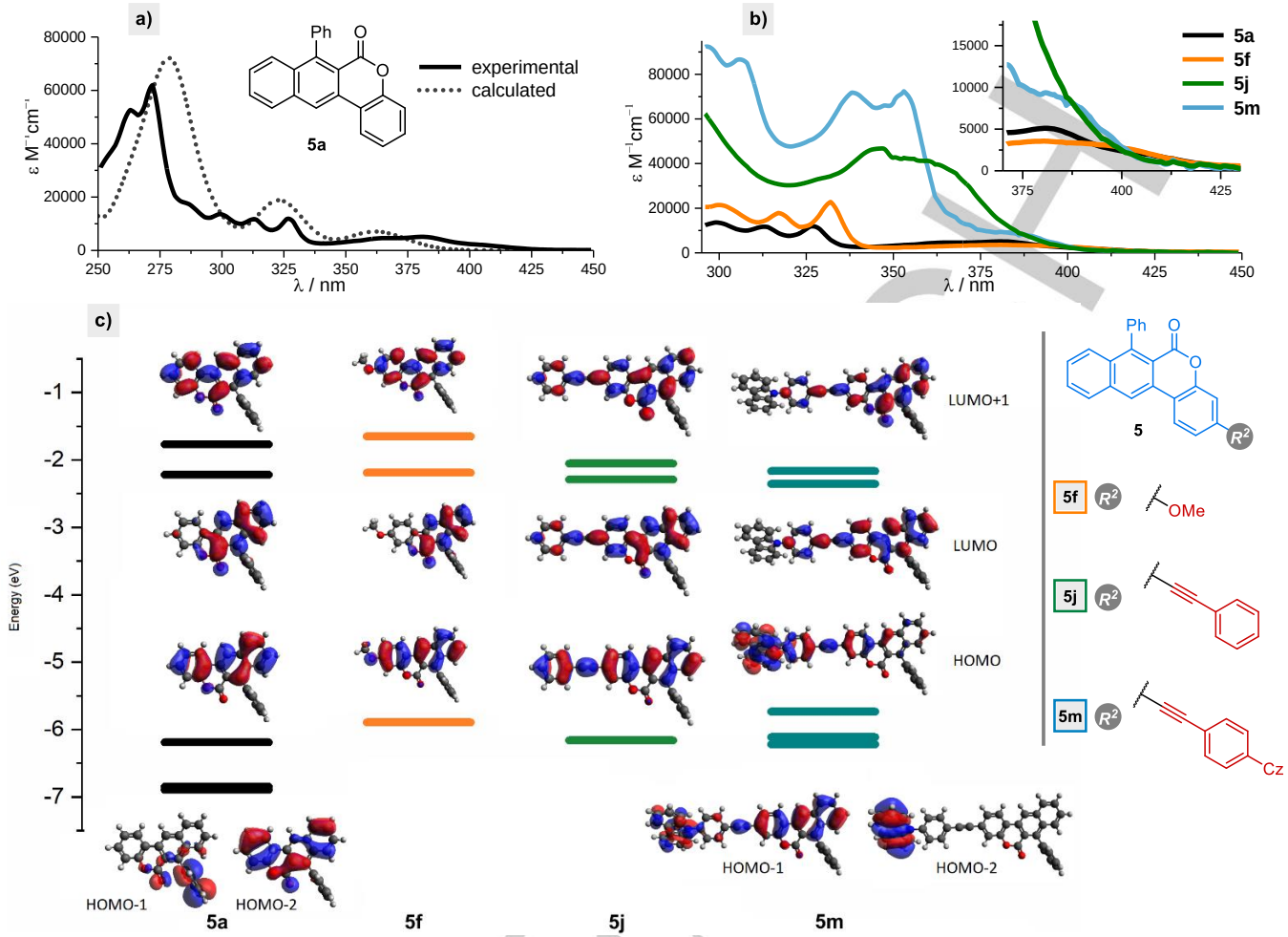


**Figure 2.** a) Measured and calculated absorption spectra of PC **5a**. b) Extinction coefficients of PC **5a**, **5f**, **5j** and **5m** measured in acetonitrile. c) Representation of selected frontier molecular orbitals of PC **5a**, **5f**, **5j** and **5m** and relative energies. Cz = carbazole **Figure 4.** a) Measured and calculated absorption spectra of PC **5a**. b) Extinction coefficients of PC **5a**, **5f**, **5j** and **5m** measured in acetonitrile. c) Representation of selected frontier molecular orbitals of PC **5a**, **5f**, **5j** and **5m** and relative energies. Cz = carbazole.

To get insight into the electronic transitions responsible for the absorption, we used time-dependent density functional theory (TD-DFT) at the B3LYP/6-311+g(d,p) level of theory, including a polarizable continuum model (PCM) of water, as representative case for polar solvent.[13] As shown in Figure 2c (black levels), the HOMO, LUMO and LUMO+1 orbitals are localized on the NTC core of **5a**, with no contribution of the phenyl group at 7 position, due to its perpendicular geometry with respect to the plane described by the NTC scaffold, in agreement with its X-ray crystal structure (Table 1).[14] These three orbitals are involved in the two low energy transitions calculated with TD-DFT. In particular, the HOMO→LUMO transition provides the highest contribution (91%, Table S7 in SI) to the lowest energetic one, predicted at 362 nm (Figure 2a, dotted line) and characterized by an oscillator strength of 0.0693 (roughly corresponding to an ε of 5×103 $M^{-1}cm^{-1}$), in fair agreement with the longer wavelength experimental ab-sorption discussed above (λ = 380 nm, ε = 5100 $M^{-1}cm^{-1}$). The second lowest energetic transition is predicted at 323 nm (oscillator strength 0.1848, again in excellent agreement with the experimental data) and is characterised by a major HOMO→LUMO+1 contribution setting to 71%. It is worth mentioning that a third intense transition is predicted at lower wavelengths (λ = 281 nm. oscillator strength = 0.5346, ε ca 4×104$M^{-1}cm^{-1}$, in fair agreement with an experimental absorption centred at 272 nm with ε = 61500); this transition comes from different contributions from the frontier orbitals, including filled orbitals cantered on the phenyl group in 7 position, such as the HOMO-2. Substitutions at position 7 have relatively small influence on the PCs absorption spectra (Figure S69 in SI). The absence of the phenyl ring, as for **5c**, involves a shift to shorter wavelengths (about 10 nm). **5b** bearing a fluorine at the *orto*-position of the phenyl ring showed a spectrum that mirrors the one of **5a**. The introduction of an electron withdrawing bromine (**5d**) or a triflate (**5e**) at position 3, is reflected in a slight shift of the peaks at longer wavelengths and the absorption decreases in the λ > 400 nm region. On the contrary, compounds **5f** and **5g**, bearing electron donating methoxy or hydroxy group have enhanced absorption in the visible region, in particular **5f** (Figure 2b, orange

line) being the most absorbing in the whole series of PCs. Interestingly, this behaviour was consistent with calculated absorptions by TD-DFT (Table S7 in SI). Indeed, focusing on the two less energetic transitions as discussed for **5a**, no major changes were observed in the series of PCs **5a**-**d**. The similar absorption features calculated are consistent with the minor changes observed in LUMO and LUMO+1 energy in this series (Figure S89 in SI), that are mainly ascribable to the electronic character of the groups on the NTC scaffold. Interestingly, as observed in the experimental data, effects are observed for **5f** and **5g**, where a 0.2-0.3 eV raising in the energy of the HOMO orbitals is observed, consistent with the electron-donating character of the methoxy and hydroxy group at position 3. The calculated absorption spectra of these two PCs show a red shift to 387 and 385 nm for **5f** and **5g**, respectively, in agreement with the experimental values at 393 and 391 nm. A different scenario in absorption properties is observed by introducing conjugation at position 3 (compounds **5h**-**m**).

**Table 2.** Excited- and Ground-State Photoredox Properties Summary.

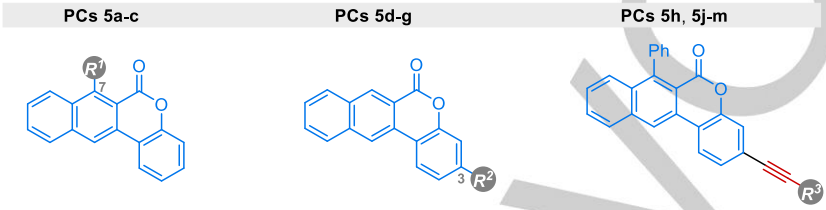


| PC | $\lambda_{max}$em. (nm) | $E_{0,0}$ [a] (eV) | QY % | τ (ns) | E [b] (PC/PC•⁻) | E [b] (PC•⁺/PC) | E [b] (PC*/PC•⁻) | E [b] (PC•⁺/PC*) |
|---|---|---|---|---|---|---|---|---|
| **5a, ($R^1$ = 7-Ph)** | 421 | 3.29 | 4 | 1.44 | -1.74 | 1.75 | 1.55 | -1.54 |
| **5b, ($R^1$ = 7-*o*-F)** | 421 | 3.30 | 9 | 2.07 | -1.68 | 1.81 | 1.62 | -1.49 |
| **5c, ($R^1$ = 7-H)** | 411 | 3.35 | 8 | 3.86 | -1.67 | 1.80 | 1.68 | -1.55 |
| **5d, ($R^2$ = 3-Br)** | 421 | 3.26 | 5 | 1.49 | -1.61 | 1.78 | 1.65 | -1.48 |
| **5e, ($R^2$ = 3-OTf)** | 413 | 3.29 | 4 | 0.81 | -1.55 | 1.86 | 1.74 | -1.43 |
| **5f, ($R^2$ = 3-OMe)** | 462 | 3.07 | 20 | 7.78 | -1.76 | 1.47 | 1.31 | -1.60 |
| **5g, ($R^2$ = 3-OH)** | 461 | 3.07 | 12 | 8.50 | -1.89 | 1.44 | 1.18 | -1.63 |
| **5h, ($R^3$ = TMS)** | 426 | 3.22 | 15 | 2.53 | -1.71 | 1.73 | 1.51 | -1.49 |
| **5j, ($R^3$= Ph)** | 434 | 3.20 | 17 | 3.34 | -1.70 | 1.64 | 1.50 | -1.56 |
| **5k, ($R^3$= *p*-CN-Ph )** | 427 | 3.23 | 23 | 3.05 | -1.58 | 1.69 | 1.65 | -1.54 |
| **5l, ($R^3$= *p*-OMe-Ph )** | 449 | 3.15 | 16 | 4.21 | -1.65 | 1.44 | 1.50 | -1.71 |
| **5m, ($R^3$= *p*-Cz-Ph)** | 459 | 3.18 | 6 | 2.49 | -1.59 | 1.35 | 1.59 | -1.83 |

[a] Estimated by emission onset. [b] All potentials in V vs SCE. Measurements were performed in ACN (See SI for details). TMS = trimethylsilyl; Cz = carbazole.

Summarizing, the effects can be discussed as follows: i) for all compounds **5h**-**m** the extinction coefficient increases significantly (See e.g. **5j** and **5m** in Figure 2b); ii) the simple addition of a triple bond in position 3 (**5h**) is sufficient to shift the peaks 15 nm towards the visible even if the HOMO and LUMO shape and energy are not significantly affected (calculated λ3 = 369 nm, Table S7 and Figure S89 in the SI); conversely, the presence of the triple bond significantly lowers the energy of the LUMO+1 orbital: moving from -1.771eV for **5a**, to -2.053 and -2.067 eV for **5j** and **5m**, respectively (Figure 2c). Thus, causing a red shift of the second less energetic transition at 323 for **5a**, to 371 and 387 nm for **5j** and **5m**, respectively; iii) the further conjugation with a phenyl group increases the red shift of the absorption as observed for **5j**, **5k**, **5l**, **5m** with a less energetic peak at 385-390 nm, this effect being ascribed to the increase in the HOMO energy, thus affecting also the less energetic transition. Besides **5m**, the presence of substituents on the phenyl group conjugated to the triple bond does not impact on the type of orbitals involved in the transitions, although changes the relative energy according to electronic factors (Figure S89 in SI); iv) **5m** has the most red-shifted absorption (Figure 2b, azure line) ascribed to a distinctive HOMO higher in energy and located predominantly on the carbazole moiety, suggesting an intramolecular charge transfer contribution.

**Excited state analysis.** In organic PCs, the first singlet excited state (S1) is the most likely to react in bimolecular reactions to perform photoinduced electron transfer (PET).[15] Therefore, the

characterization of the excited state in terms of its energy, its decay pathway and its lifetime, is instrumental to predict its reactivity.[15b] Indeed, high energy excited state means the possibility of applications in a number of diverse PET reactions. Long lifetime will match with greater chances of encountering the desired reactant and the higher the fluorescence quantum yield, the greater the likelihood of PET happening in the singlet excited state.[6c] We started analysing **5a** looking at the modifications of S1 properties caused by the different substitutions performed on the PC scaffold. PC **5a** has an emission maximum at 421 nm, consistent with an excited state energy of 3.29 eV, an emission quantum yield (QY) of 4% and an excited state lifetime of 1.44 ns (Table 2). Removing the phenyl ring in position 7 (**5c**) determines an emission shift of 10 nm to shorter wave-lengths with an excited state energy of 3.35 eV, the highest in the series. The more compact core led to longer lifetime (3.86 ns) and higher QY (8%). On the other side, substitutions with electron withdrawing groups at different positions of the NTC core did not alter significantly the properties of **5a** maintaining lifetime and QY to suitable levels. Notably, PCs **5f** and **5g**, bearing electron-donating groups (Table 2), showed an increased QY to 12% for **5g** and to 20% for **5f** and a lifetime extension to 8.50 ns and 7.78 ns, respectively. Hence, these PCs are very good candidates towards demanding reductive PET processes. Finally, the increasing of the conjugation by a triple bond in compounds **5h**-**5m** also showed promising properties in between **5a** and **5f**-**5g**. The emission maximum was observed in a range from 427 nm (**5k**) to 459 nm (**5m**) with associated excited state energies between 3.18-3.23 eV. Quantum yield was observed in the range 15% to 23%, increased with respect to **5a**. The lifespan of the excited state was generally longer than 2 ns with a maximum for **5l** reaching 4.21 ns.

**Redox properties analysis.** One of the advantages of the NTC PCs **5**, able to absorb at the border of visible light, is the associated wide redox window which allows both highly demanding reductive and oxidative quenching cycles. Looking at compound **5a**, the PC exhibited a reversible reduction at -1.54 V vs SCE ($PC^{\bullet+}/PC^*$) and an oxidation ($PC^*/PC^{\bullet-}$) at 1.55 V vs SCE. These values are well suited for a large variety of different photoreactions requiring strong oxidative or reductive power. Modulating the substituents within the NTC core, it is possible to reach the most negative values for E ($PC^*/PC^{\bullet-}$) with electron donating groups in position 3, as in the case of **5f** with -1.60 V vs SCE, **5g** -1.63 V. Highly negative values were also registered for PCs with extended conjugation ranging from -1.49 V for **5h** up to a remarkable -1.83 V for **5m** (Table 2). Moving to the $PC^*/PC^{\bullet-}$ oxidative process we immediately discern the wider variability of the PCs covering the window from 1.18 V for **5g** to 1.74 V for **5e**. As observed for the potential regarding ($PC^*/PC^{\bullet-}$), the electron-donating ability of the substituents have a clear effect on the redox potentials, increasing the energy of the HOMO. Interestingly, addition of electron withdrawing groups such as the case of **5b**, **5d**, **5e** and **5k** stabilizes the HOMO of the PCs bringing the oxidation potential above 1.62 V.

**Analysis of the Photocatalytic Performances.** After having established general structure-property relationships across the 12 PCs, we first evaluated their photocatalytic performances with respect to the Povarov-type addition of *N,N*-dimethylaniline **6a** to phenylmaleimide **7** (Scheme 3). The choice of this photoreaction was made on the bases of three main considerations: in first instance (i) to relay on a well-known reaction mechanism where the PC is involved in two catalytic steps: the oxidation of **6a** (by PC*) and the reduction of $O_2$ (by $PC^{\bullet -}$).

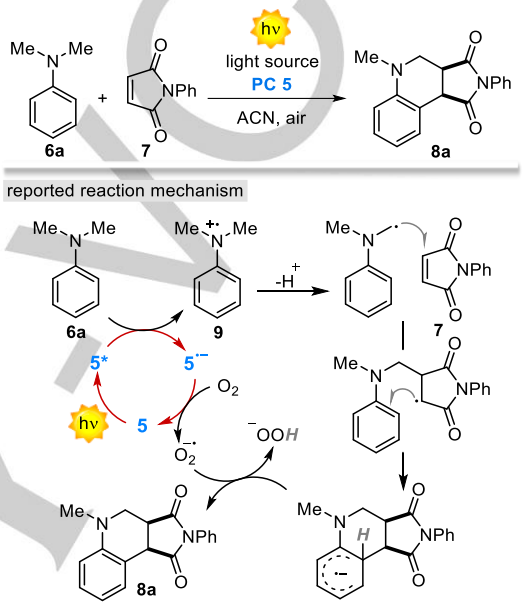


**Scheme 3.** Povarov-type addition of N,N-dimethylaniline **6a** to phenylmaleimide **7** and reported reaction mechanism.

The reported mechanism has been studied for both metal[16] and organic PCs,[17] facilitating comparisons; (ii) to assess the physicochemical stability of NTCs under the reaction conditions. The presence of oxygen and hydrogen peroxide under basic conditions has been documented to be detrimental for the stability of different PCs[18] and finally (iii) for the redox potential of **6a** ($E_0$ $\mathbf{6a}^{\bullet+}/\mathbf{6a}$ = +0.80 V vs SCE) and $O_2$ ($E_0$ $O_2/O_2^{\bullet-}$ = -0.64 V vs SCE),[19] which are within the operational windows of the 12 developed PCs, thus ensuring their comparison. Mechanistically, under light irradiation the PC **5** reaches an electronically excited state **5*** which is able to oxidize **6a** to the corresponding radical cation, while generating the strong reductant **5** radical anion (-1.74 V vs SCE). At this stage, $5^{\bullet-}$ reduces molecular oxygen, thus closing the photocatalytic cycle. As reported, the first step of the reaction (Scheme 3) involves a reductive quenching of the PC yielding its reduced form and the radical cation **9**.[20] As expected *N,N*-dimethylaniline **6** can efficiently quench **5***. The rate of this process was evaluated for PCs **5a**-**m** by Stern-Volmer plot (Figure 3). Considering a pure dynamic quenching, the slope ($K_{PC}$) of the Stern-Volmer plot is defined as: $K_{PC} = k_q\tau_{PC}$, where $k_q$ is the bimolecular rate constant and $\tau_{PC}$ the excited state lifetime of the photocatalyst.[21] Interestingly, the $k_q$ of the different PCs **5** (Table

S3 in SI) fall in a narrow range from 1.2 to 3.5 x $10^{10}$ $M^{-1}s^{-1}$, ascribable to diffusion controlled processes. As a result the differences among the quenching slopes ($K_{PC}$) mainly reflect the excited state lifetime τ (Table 2). In fact, **5f** and **5g**, having a τ of 7.78 and 8.5 ns, respectively, exhibited the steepest slopes. PCs with an extended conjugation such as **5h**-**5l** with a τ ranging from 15 to 23 ns also showed an efficient quenching. The trend was confirmed also considering the PCs with the shortest τ, such as **5d** and **5e**, which revealed the least efficient. A second correlation was found with respect to the QY. All the PCs **5** with a quantum yield higher than 8% showed the fastest quenching.

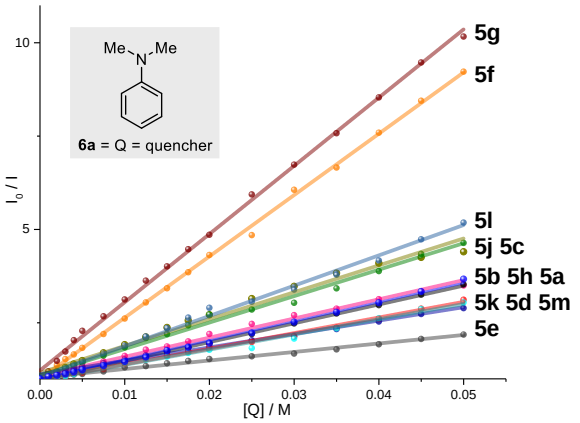


**Figure 3.** Stern-Volmer quenching between PCs **5** and *N,N*-dimethylaniline **6a** in ACN.

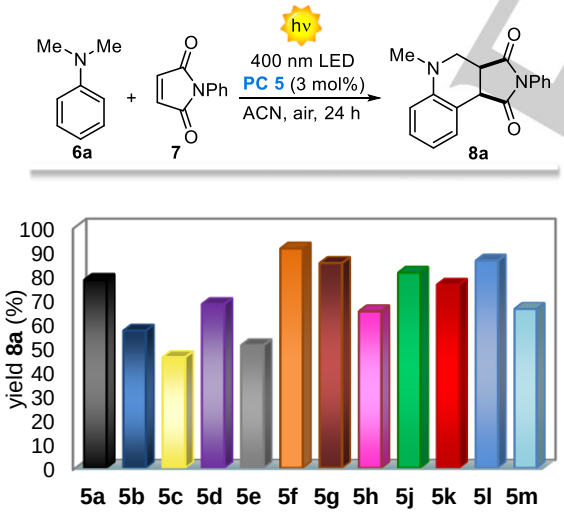


**Figure 4.** Observed performances of the PCs 5 for the reaction between *N,N*-dimethylaniline **6a** and phenylmaleimide **7**. The reported isolated yields represent the media of two independent runs.

We next examined the photocatalytic performances of the 12 PCs in the Povarov-type reaction between *N,N*-dimethylaniline **6a** and phenylmaleimide **7** monitoring the yields of product **8a** after 24 h reaction time (Figure 4). All the reactions were performed under the reaction conditions previously reported for eosin Y photocatalyst.[17] The best performing PCs were **5f** and **5g** which furnished the product **8a** in 91% and 86% yield respectively – in perfect agreement with the quenching experiments. As predicted, also PCs **5l** showed excellent performances with 85% yield. PCs **5a**, **5d**, **5j** and **5k** furnished the product in good yields spanning from 76% to 80%.

**Table 3.** Observed performances of the diverse PCs **5** beyond the state-of-the-art synthetic applications.

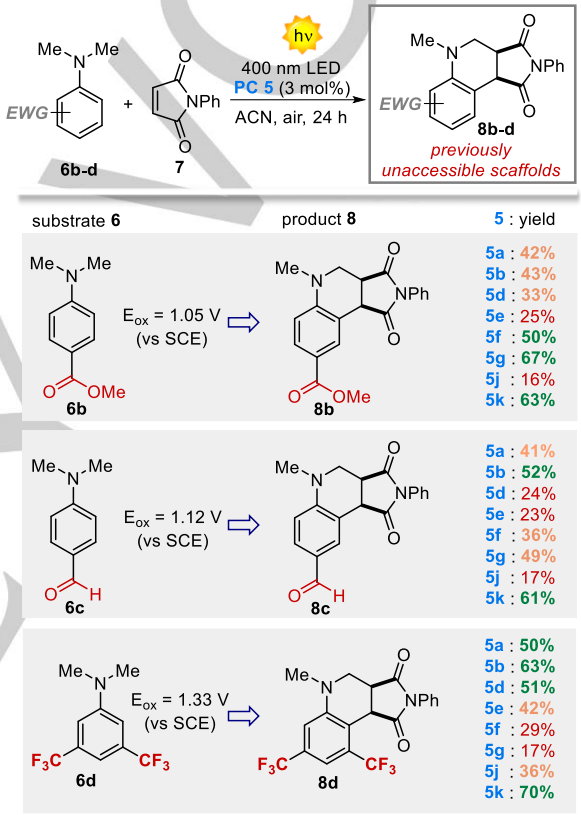


In these cases, the fastest quenching is observed for **5j**, supported by Stern-Volmer experiments and reflected in a τ of 3.34 ns and a high extinction coefficient at the operative wavelength (400 nm). The least performing PCs were **5e** and **5c**, with 51% and 46% yield, respectively. While **5e** performances were predicted by the lowest quenching constant of the series, **5c** performances were affected by the lowest absorption among the 12 PCs. Other PCs **5b**, **5d**, **5h** and **5m** gave average performances from 57% to 66% yield. It is worth mentioning that PCs **5f**, **5g** and **5l** outcompete the previously reported results for eosin Y[17] and $Ru(bpy)_3$,[16] which furnished **8a** in 82% and 83% yield. Next, we selected substrates **6b**-**d**, because of their high oxidation potentials ($E_{ox}$ = 1.05-1.33 V vs SCE, CV spectra in SI). The incipient radical cations, involved in the initial PC reductive quenching (Scheme 3), are destabilized by EWGs, thus hampering the use of these substrates when . These types of *N,N*-

dimethylanilines are beyond the state-of-the-art synthetic applications reported so far, catalysed by Ru-,[16] Cu-,[22] Co,[23] Ir,[24] Pt-complexes,[25] eosin Y17 and different supported metal oxides including $TiO_2$.[26] In all these cases only halogens were partially tolerated as EWGs. When a different EWG was placed on the aromatic ring it completely shut down the reactivity of the system and no reaction was observed. We started evaluating **6b**, bearing an ester group at the *para*-position ($E_{ox}$ = 1.05 vs SCE). We were pleased to note that different PCs were able to catalyse this reaction. Interestingly, as for the reaction with simple *N,N*-dimethylaniline **6a** two of the best performances were registered for **5f** and **5g**, with 50% and 67% yield respectively. Remarkably, the highly oxidant PC **5k** furnished the product in 63% yield. Moving to a more difficult substrate, **6c** was selected not only for the higher oxidation potential ($E_{ox}$ = 1.12 V vs SCE), but also for the presence of an aldehyde moiety particularly unstable under oxidative conditions. Gratefully, different PCs were able to drive this particular difficult reaction. In particular PCs **5b** and **5k**, characterized by high excited state reduction potentials delivered **8c** in 52% and 61% yield, respectively. Additional experiments were carried out with **6d** ($E_{ox}$ = 1.33 vs SCE), bearing two $CF_3$ groups at the *meta*-positions. Remarkably, several PCs were able to catalyse this photoreaction. The most oxidant PCs exhibited the best performances with **5k** furnishing **8d** in 70% yield. It is interesting to note how PCs **5f** and **5g** ($PC^*/PC^{\bullet -}$ = 1.31 and 1.18 V, respectively) showed inferior performances while moving from **6a**-**b** to the more oxidant substrate **6d**. This indicating an increased impact of the excited state oxidative power ($5^*/5^{\bullet -}$) while moving towards the thermodynamic oxidation limits of the PC. These experiments confirmed how the identification of novel PCs with wide redox windows can open the way to previously inaccessible reactivity.

**Synthetic Applications and Comparison of the Photocatalytic Performances.** Encouraged by the results obtained for previously unreactive substrates, we decided to evaluate PCs **5** in diverse photochemical transformations. Selected PCs were tested under a decarboxylative Giese-type addition between protected proline **9a** and dimethyl maleate **10** (Scheme 4). This reaction, firstly reported by MacMillan and co-workers,[27] has been widely used as an evaluation probe for the synthetic performances of diverse photocatalytic systems, including: Ir-based PCs,[27] acridiniums[8c] and cyanoarenes.[6c] What makes this transformation particularly difficult to be efficiently catalysed is the need of an optimal balance between the oxidative excited state properties of the PC and the reductive power of the corresponding radical anion. This ensuring: (i) an efficient decarboxylation step – with a PC* reducing quenching (**9b**-Cs $E_{ox}$ = 0.95 V vs SCE)[27] – which generates the reactive α-amino radical **12** and (ii) a fast reduction of the formed α-acyl radical **13** ($E_{red}$ = - 0.60 V vs SCE) – with a $PC^{\bullet -}$ oxidation step – which closes the photocatalytic cycle. It is worth mentioning that diverse Ir-based and cyanoarenes PCs with competent redox properties turned out to be inefficient PCs for this type of transformation.

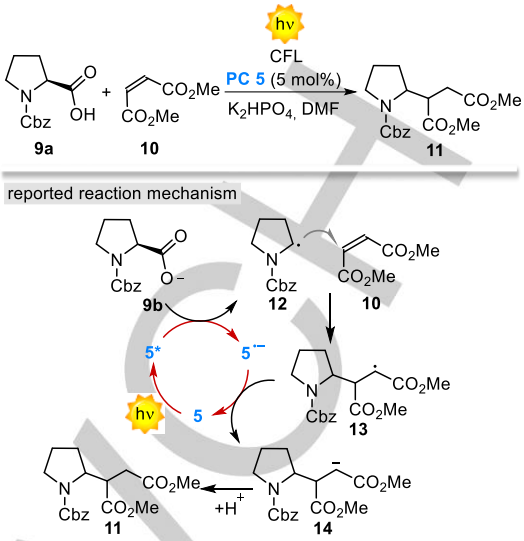


| entry[a] | PC | yield %[b] |
|---|---|---|
| 1 | 5a | 66 (63) |
| 2 | 5b | 48 |
| 3 | 5d | 53 |
| 4 | 5e | 12 |
| 5 | 5f | 62 |
| 6 | 5k | 77 (75) |
| 7 | 5m | 72 (70) |
| 8[c] | (Mes-4MeOAcr-2MeOPh)+ | 73 |
| 9[d] | 4CzIPN | 80 |
| 10 | eosin Y | - |

[a] Reactions in DMF (0.5 mL) for 20h on a 0.2 mmol scale illuminated by CFL bulb using PCs **5** (5 mol%), SI for details. [b] Yield of **11** determined by $^1$H NMR analysis of the crude mixture using trimethoxybenzene as internal standard. Values in parenthesis refer to isolated yields.

[8c, 27] A reduced PC oxidative power resulted in drastic reactivity loss. In our initial attempt we used 5 mol% of **5a**, under the reaction conditions described by MacMillan and co-workers.[27] Interestingly, by using readily available CFL bulbs, the expected addition product **11** was obtained in 63% yield. Having in hand other PCs with higher oxidation potentials we explored their catalytic performances under the same reaction conditions. Quite unexpectedly, PCs **5b** and **5d** furnished the product in modest yield, 48% and 53%, respectively (Table 4, entries 2 and 3). Inferior results were obtained for **5e** (Table 4, entry 4), in agreement with his very short excited state lifetime of 0.81 ns (Table 1). PC **5f**, having inferior excited state oxidative power ($\mathbf{5f}^*/\mathbf{5f}^{\bullet -}$ = 1.31 V) and superior τ (7.78 ns) showed superior performances with 62% yield (Table 4, entry 5).

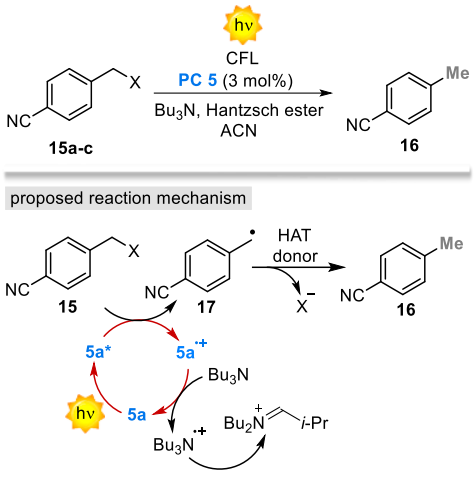


**Scheme 5.** Direct light-driven dehalogenation reaction of benzyl halides **15a-c** – Proposed reaction mechanism.

Finally, PCs with an extended conjugation such as **5k** and **5m** efficiently catalysed this reaction with 75% and 70% yield, respectively. In particular **5k** with a **5k*/5k•-** = 1.65 and τ = 3.05 resulted the best of the series (Table 3, entry 6). Selected metal-based PCs were also compared under the same reaction conditions (Table 3, entries 8-10). The only PC giving some conversion was $Ir(dFppy)_3$ while the other Ru- and Ir-based PCs proved completely inefficient in agreement with previous studies.[27] To further evaluate the operational limits of PCs **5** we selected diverse benzyl halides **15** (Scheme 5). Following the reports by Stephenson and co-workers on similar dehalogenation reactions,[28] we assumed the reaction to proceed through a PC reductive quenching cycle. After the initial reduction of the PC* to its radical cation, with the irreversible formation of the benzylic radical **17**. The presence of tributylamine (*n*-$Bu_3N$) is required to regenerate the PC ground state, thus closing the photocatalytic cycle. Preliminary Stern-Volmer quenching experiments indicated that, **5a*** can be quenched by both the benzyl halide and the amine. This indicates the feasibility of two alternative yet convergent reaction mechanisms.[29] The strong oxidative and reductive power of the developed class of PCs **5**, allows both reductive and oxidative quenching cycles to be operative (Figure 1), with definite advantages on the overall reactivity of the system. When PC **5a**, was irradiated under 400 nm light the benzyl iodide **15a** and benzyl bromide **15b** were efficiently reduced to the corresponding toluene derivative **16** in 72% and 80% yield respectively (Table 5, entry 1 and 2).

**Table 5.** Observed performances of the diverse PCs **5** for the direct light-driven dehalogenation reaction of benzyl halides **15a-c**.

| entry | 15, X | $E_{red}$ (V vs SCE)[b] | PC | (16) yield |
|---|---|---|---|---|
| **1** | 15a, I | -1.25 | **5a** | 82 (72) |
| **2** | 15b, Br | -1.64 | **5a** | 82 (80) |
| **3** | 15b, Br | -1.64 | **5e** | 9 |
| **4** | 15b, Br | -1.64 | **5f** | 58 (67) |
| **5** | 15b, Br | -1.64 | **5l** | 62 |
| **6** | 15b, Br | -1.64 | **5m** | 46 |
| **7** | 15c, Cl | -1.81 | **5a** | 15 |
| **8** | 15c, Cl | -1.81 | **5f** | 48 (47) |
| **9** | 15c, Cl | -1.81 | **5l** | 54 (51) |
| **10** | 15c, Cl | -1.81 | **5m** | 45 |
| **11** | 15c, Cl | -1.81 | eosin Y | - |
| **12** | 15c, Cl | -1.81 | $Ru(bpy)_3$ | - |
| **13** | 15c, Cl | -1.81 | $Ir(ppy)_3$ | <5 |
| **14** | 15c, Cl | -1.81 | $Ir(dFppy)_3$ | 19 |

[a] Reactions in ACN at room temperature for 16 h on a 0.2 mmol scale under illumination by 400 nm LED strips using PCs **5** (3 mol%), SI for details. Hantzsch ester as HAT donor. [b] Yield of 16 determined by GC-FID analysis of the crude mixture using mesitylene as internal standard. Values in parenthesis refer to isolated yields.

As expected, the less reductant PC **5e** showed much inferior results, while more electron-rich and more reductant PCs **5f** and **5m** performed well delivering **16** in 67% and 62% yield, respectively (Table 5, entries 5 and 6). Unexpectedly, PC **5m** with the highest excited state reduction potential (**5m•+/5m*** = -1.83 V vs SCE) furnished **16** in 46% yield. We next examined benzyl chloride **15b**, which has a reduction potential of -1.81 V vs SCE (CV spectrum in SI). Importantly, benzyl chlorides are generally unexpansive and readily available starting materials but their use in photocatalysis is often restricted by their difficult single-electron reduction. Notably, when the reaction was performed in the presence of **5a** product **16** was obtained in 15% yield. This prompted us to screen all the PCs we developed with respect to this unprecedented transformation. Only the most reducing PCs showed some conversion, with **5f**, **5l** and **5m** furnishing promising results, 47% and 51% yield, respectively (Table 5, entry 8 and 9). In all the other cases product traces or no reaction was observed. The fact that only the most reductant PCs **5** were able to catalyse this reaction points to an oxidative quenching mechanism. The difficulty in catalysing this reaction was further evaluated with respect to diverse metal-based PCs (Table 5, entries 11-13). Only the highly reductant $Ir(dFppy)_3$ furnished the product to some extent (19% yield). It is worth mentioning that the only way to directly generate this type of radical starting from benzyl chloride[30] under photochemical conditions is under deep-UV photochemistry.[31]

**Table 6.** Direct light-driven dehalogenation reaction of methyl 4-iodobenzoate **18**.

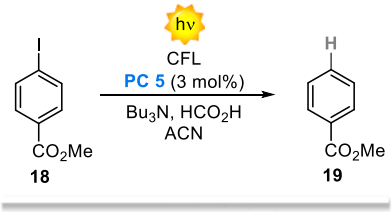


| entry | PC | yield % |
|---|---|---|
| **1** | **5a** | 86 (83) |
| **2** | **5d** | 16 |
| **3** | **5e** | 13 |
| **4** | **5f** | 81 |
| **5** | **5m** | 96 (93) |
| **6** | eosin Y | - |
| **7** | $Ru(bpy)_3$ | <5 |
| **8**[c] | $Ir(ppy)_3$ | 92 |

[a] Reactions in ACN at room temperature for 20h on a 0.1 mmol scale under illumination by CFL bulb and using PCs **5** (3 mol%), SI for details. Formic acid as HAT donor. [b] Yield of **19** determined by $^1H$ NMR analysis of the crude mixture using trimethoxybenzene as internal standard. Values in parenthesis refer to isolated yields. [c] Reference result as in reference 28b.

Prompted by the unprecedented results obtained for the reduction of benzylic chlorides, we next examined a de-iodination of arenes. We selected methyl 4-iodobenzoate **18** whose the highly negative reduction potential ($E_{red}$ = -1.96 V vs SCE, CV spectrum in SI) will have challenged the photoredox properties of the developed PCs. In this case the reactions were performed applying the conditions reported by Stephenson and co-workers.[28b] Interestingly, PC **5a** performed smoothly delivering product **19** in 83% yield after 20h irradiation (Table 6, entry 1). Less reducing PCs, such as **5d** and **5e** gave **19** in poor yields (16% and 13% respectively). Contrarily, highly reducing PC **5f** and **5m** produced **19** in 81% and 93% yield, respectively (Table 6, entries 4 and 5). As expected, $Ru(bpy)_3$ was completely inefficient (entry 6) while the more reductant $Ir(ppy)_3$ complex furnished the product in high yield (entry 7). It should be noted that this type of reactions can be catalysed only by precious highly reductant Ir-complexes[28b] or trough consecutive visible light-induced electron transfer processes.[32] In this sense the use of NTC photocatalysts represent a new viable option.[33]

## Conclusion

In conclusion, we have identified naphtochromenones as a new class of powerful organic photoredox catalysts. A versatile synthetic route was developed which allowed the synthesis of the PCs at gram scale, making the use of these PCs affordable and more sustainable with respect to classical Ru- or Ir-based PCs. As demonstrated, the NTC core can be easily tuned by employing diverse starting building blocks or through straightforward functionalization. Furthermore, exploiting an absorption across UV- and visible-light, these PCs are characterized by a wide redox window up to 3.35 eV, outcompeting all the PCs relaying on visible light absorption. As demonstrated, their powerful exited (from -1.83 to 1.74 V) and ground state (from -1.89 to 1.86 V) redox potentials allow to access both challenging oxidative and reductive light-driven transformations. Structure-property relationship were carefully assessed with respect to 12 different scaffolds and supported by DFT calculations. Allowing further uses and modifications towards the intended purpose. Regarding the synthetic performances, we identified **5a** as a versatile PC, able to drive a variety of light-driven processes diverse in nature (Povarov-type cycloaddition = 41-83% yield, Giese addition = 63% yield, benzyl chloride dehalogenation = 15%, aryl iodide dehalogenation = 83% yield). Modification at position 7 (**5b**, **5c**) did not result in any particular improvements, highlighting the need of the phenyl ring to ensure higher absorption under visible light. On the other hand, modification at position 3 (PCs **5d**-**g**) resulted very effective, with PC **5f** being particularly suitable in performing challenging photoreactions where highly reductant excited states are required (benzyl chloride dehalogenation = 47% yield, aryl iodide dehalogenation = 81% yield). Finally, PCs with extended conjugation (**5h**-**5m**) showed complementary performances, with **5k** higly effective under reductive quenching cycles (Povarov-type cycloaddition = 61%-80% yield, Giese addition = 75% yield), and **5l** and **5m** resulting the best PCs for the reduction of benzyl chlorides and aryl iodides (51% and 93% yield, respectively). With affordable synthetic protocols, well-defined structure property relationship and preliminary synthetic applications, the naphthochromenone PCs presented here are a new viable opportunity towards the development of unprecedented light-driven transformations.

## Experimental Section

Coumarin **2a** (6.58 g, 5 equivalents, 45 mmol) was introduced into a 250 mL round-bottom flask under $N_2$ atmosphere and dissolved with 150 mL of degassed toluene. Then, 2-methylbenzophenone **1a** (1.65 mL, 1 equivalent, 9 mmol) was added in one portion and the solution was further bubbled with $N_2$ for 10 minutes. The obtained solution was pumped into two parallel photoreactors and irradiated by a 9W 365nm bulb with a residence time of 35 minutes (for an overall time of 44 h). The product solution was collected into a 250 mL round-bottom flask. Subsequently, the solvent was removed by rotary evaporation and the crude subjected to flash column chromatography on silica gel (9:1 Hexane/EtOAc) yielding pure **3a** (white solid), as a single diastereoisomer in 99% yield (3.1 g, 9 mmol). The excess of coumarin **2a** was recovered after flash column chromatography.

## Acknowledgements

This work was supported by the CariParo Foundation with the AMYCORES starting grant 2015 to L.D.. A. V.–P. thanks the University of Padova for the Seal of Excellence @unipd PLACARD fellowship. AS thanks the university of Padova and the Department of Chemical Sciences for funding (P-DiSC #10BIRD2018-UNIPD). Stefano Mercanzin, Mauro Meneghetti and Alberto Doimo are acknowledged for technical assistance.

**Keywords:** photoredox catalysis • organic catalyst • synthetic applications • structure-property relationship • radical chemistry

[1] a) L. A. Weinstein, J. Loomis, B. Bhatia, D. M. Bierman, E. N. Wang, G. Chen, *Chem. Rev.* **2015**, *115*, 12797–12838; b) J. Gong, C. Li, M. R. Wasielewski, *Chem. Soc. Rev.* **2019**, 48, 1862-1864; c) Y. Wang, H. Suzuki, J. Xie, O. Tomit, D. J. Martin, M. Higashi, D. Kong, R. Abe, J. Tang, *Chem. Rev.* **2016**, *116*, 9664–9682; d) G. J. Hedley, A. Ruseckas, D. W. Samuel, *Chem. Rev.* **2017**, *117*, 796–837.

[2] a) D. M. Schultz, T. P. Yoon, *Science*, **2014**, *343*, 1239176-1239184; b) D. Ravelli, D. Dondi, M. Fagnoni, A. Albini, *Chem. Soc. Rev.* **2009**, *38*, 1999–2011; c) L. Buzzetti, G. E. M. Crisenza, P. Melchiorre, *Angew. Chem. Int. Ed.* **2019**, *58*, 3730-3747.

[3] a) J. C. Theriot, C. H. Lim, H. Yang, M. D. Ryan, C. B. Musgrave, G. M. Miyake, *Science*, **2016**, *352*, 1082–1086; b) N. Corrigan, S. Shanmugam, J. Xu, C. Boyer, *Chem. Soc. Rev.* **2016**, *45*, 6165–6212.

[4] a) L. Marzo, S. K. Pagire, O. Reiser, B. König, *Angew. Chem. Int. Ed.* **2018**, *57*, 10034–10072; *Angew. Chem.* **2018**, 130, 10188–10228; b) C. Michelin, N. Hoffmann, *Curr. Opin. Green Sustain. Chem.* **2018**, *10*, 40–45; c) T. Bach, P. Hehn, *Angew. Chem. Int. Ed.* **2011**, *50*, 1000–1045; *Angew. Chem.* **2011**, 123, 1032-1077.

[5] a) C. K. Prier, D. A. Rankic, D. W. C. MacMillan, *Chem. Rev.* **2013**, *113*, 5322–5363; b) A. Hossain, A. Bhattacharyya, O. Reiser, *Science*, **2019**, 364, eaav9713; c) M. H. Shaw, J. D. A. Twilton, D. W. C. MacMillan *J. Org. Chem.* **2016**, *81*, 6898–6926; d) R. C. McAtee, E. J. McClain, C. R. J. Stephenson, *Trends in Chemistry*, **2019**, *1*, 111–125; e) N. A. Romero, D. A. Nicewicz, *Chem. Rev.* **2016**, *116*, 10075–100166; f) K. L. Skubi, T. R. Blum, T. P. Yoon, *Chem. Rev.* **2016**, *116*, 10035-10074; g) D. P. Haria, B. König, *Chem. Commun.*, **2014**, *50*, 6688-6699.

[6] For selected recent examples see: a) R. M. Pearson, C.-H. Lim, S. M. Sartor, M. D. Ryan, H. Yang, N. H. Damrauer, G. M. Miyake. *Chem. Eur. J.* **2017**, *23*, 10962-10968; b) C. Bottecchia, R. Martín, I. Abdiaj, E. Crovini, J. Alcazar, J. Orduna, M. J. Blesa, J. R. Carillo, P. Prieto, T. Noël, *Adv. Synth. Catal.* **2019**, *361*, 945-950.

[7] For a recent example see e.g.: B. D. Ravetz, A. B. Pun, E. M. Churchill, D. N. Congreve, T. Rovis, L. M. Campos, *Nature* **2019**, *565*, 343–346.

[8] a) B. G. McCarthy, R. M. Pearson, C.−H. Lim, S. M. Sartor, N. H. Damrauer, G. M. Miyake, *J. Am. Chem. Soc.* **2018**, *140*, 5088−5101; b) M. Kim, S.–J. Yoon, S. H. Han, R. Ansari, J. Kieffer, J. Y. Lee, J. Kim, *Chem. Eur. J.* **2019**, *25*, 1829–1834; c) A. Joshi-Pangu, F. Lévesque, H. G. Roth, S. F. Oliver, L.-C. Campeau, D. A. Nicewicz, D. A. DiRocco, *J. Org. Chem.* **2016**, *81*, 7244-7249; d) E. Alfonzo, F. S. Alfonso, A. B. Beeler, *Org. Lett.* **2017**, *19*, 2989-2992; e) E. Speckmeier, T. G. Fischer, K. Zeitler, *J. Am. Chem. Soc.* **2018**, 140, *45,* 15353–15365; f) J. Lu, B. Pattengale, Q. Liu, S. Yang, W. Shi, S. Li, J. Huang, J. Zhang, *J. Am. Chem. Soc.* **2018**, 140, *45,* 13719–13725; g) F. Le Vaillant, M. Garreau, S. Nicolai, G. Gryn'ova, C. Corminboeuf, J. Waser, *Chem. Sci.* **2018**, *9*, 5883-5889; h) M. Garreau, F. Le Vaillant, J. Waser, *Angew. Chem. Int. Ed.* **2019**, *58*, 8182-8186.

[9] a) J. Mateos, A. Cherubini-Celli, T. Carofiglio, M. Bonchio, N. Marino, X. Companyó, L. Dell'Amico, *Chem. Commun.* **2018**, *54*, 6820-6823; b) J. Mateos, N. Meneghini, M. Bonchio, N. Marino, T. Carofiglio, X. Companyó, L. Dell'Amico, *Beilstein J. Org. Chem.* **2018**, *14*, 2418–2424.

[10] a) L. Dell'Amico, A. Vega-Peñaloza, S. Cuadros, P. Melchiorre, *Angew. Chem. Int. Ed.* **2016**, *55*, 3313-3317; *Angew. Chem.* **2016**, 128, 3374 – 3378; b) L. Dell'Amico, V. M. Fernández-Alvarez, F. Maseras, P. Melchiorre, *Angew. Chem. Int. Ed.* **2017**, *56*, 3304–3308; *Angew. Chem.* **2017**, 129, 3352–3356; c) S. Cuadros, L. Dell'Amico, P. Melchiorre, *Angew. Chem. Int. Ed.* **2017**, *56*, 11875-11879.

[11] For the photochemistry of benzophenone and its derivatives see: D. Ravelli, S. Protti, M. Fagnoni, *Chem. Rev.* **2016**, *116*, 9850-9913. For the photochemistry of coumarins see e.g.: a) A. Gualandi, G. Rodeghiero, E. Dell Rocca, F. Bertoni, M. Marchini, R. Perciaccante, T. P. Jansen, P. Ceroni, P. G. Cozzi, *Chem. Commun.* **2018**, *51*, 10044-10047.

[12] In this case the latter oxidative aromatization step is driven by the presence of oxygen. Control experiments performed under a nitrogen atmosphere furnished only the elimination product of type **4**.

[13] This functional allowed a good match of the calculated and experimental absorption spectra; a ca 30 nm blue shift of the calculated absorption was instead observed employing the CAM-B3LYP functional, that also lead to an overestimation of the HOMO-LUMO gap. Similar discrepancies were observed with the same functional in modelling orbital energies of conjugated polymers, see: T.M. McCormick, C. R. Bridges, E. I. Carrera, P. M. DiCarmine, G. L. Gibson, J. Hollinger, L. M. Kozycz, D. S. Seferos, *Macromolecules*, **2013**, *46*, 10, 3879-3886.

[14] The plane of the phenyl ring forms indeed a 90° dihedral angle with the plane described by the 6*H*-naphthochromen-6-one scaffold, hampering its direct conjugation.

[15] For organic photosensitizers the population of the less energetic triplet excited state could be also envisaged. For general concepts and applications See: a) V. Balzani, P. Ceroni, A. Juris, *Photochemistry and Photophysics: Concepts, Research, Applications*, 1st ed.; Wiley-VCH: Weinheim, **2014**. For selected examples see: b) A. C. Benniston, A. Harriman, P. Li, J. P. Rostron, H. J. van Ramesdonk, M. M. Groeneveld, H. Zhang, J. W. Verhoeven, *J. Am. Chem. Soc.* **2005**, *127*, 16054-16064; c) M. Yamaji, Y. Hakoda, H. Okamotoc, F. Tanid, *Photochem. Photobiol. Sci.*, **2017**, *16*, 555–563. Initial experiments performed with PC **5a** revealed the presence of a $T_1$ triplet excited state with an energy of 2.31 eV (Figure S14 in SI). The resulting $T_1$ oxidation potential is set at 0.55 eV, unable to drive the reactions herein discussed (See following synthetic applications). In agreement with the lower $T_1$ excited state potentials, compound **6a** and **7** were not able to quench **5a** $T_1$ excited state, ruling out the hypothesis of triplet state catalysed processes.

[16] X. Ju, W. Li, W. Yu, F. Bian, *Adv. Synth. Catal.* **2012**, *354*, 3561-3567.

[17] Z. Liang, S. Xu, W. Tian, R. Zhang, *Beilstein J. Org. Chem.* **2015**, *11*, 425–430.

[18] a) G. Oster, N. Wotherspoon, *J. Chem. Phys.* **1954**, *22*, 157–158; b) M. Majek, F. Filace, J. A. von Wangelin, *Beilstein J. Org. Chem.* **2014**, *10*, 981–989.

[19] P.S. Singh, D. H. Evans, *J. Phys. Chem. B*, **2006**, *110*, 637–644.

[20] Stern-Volmer quenching experiments indicate that also phenylmaleimide **7** can quench **5a***. To evaluate the feasibility of alternative mechanistic scenarios, control experiments were performed in the presence of an excess of maleimide **7 (**2 and 5 equivalents). In these cases, the yields dropped significantly from 78% to 22% and 15%, respectively. Hence, the quenching of **5*** by **7** leads to an unproductive pathway.

[21] J. R. Lakowicz, *Principles of Fluorescence Spectroscopy*, 3rd ed.; Springer: Boston, **2010**.

[22] T. P. Nicholls, G. E. Constable, J. C. Robertson, M. G. Gardiner, A. C. Bissember *ACS Catal.* **2016**, *6*, 451–457.

[23] X.-L. Yang, J.-D. Guo, T. Lei, B. Chen, C.-H. Tung, L.-Z. Wu, *Org. Lett.* **2018**, *20*, 2916–2920.

[24] F. Peng, P. Zhi, H. Ji, H. Zhao, F.-Y. Kong, X.-Z. Liang, Y.-M. Shen, *RSC Adv.* **2017**, 7, 19948–19953.

[25] A. M. Ranieri, L. K. Burt, S. Stagni, S. Zacchini, B. W. Skelton, M. I. Ogden, A. C. Bissember, M. Massi, *Organometallics,* **2019**, *38*, 1108–1117.

[26] J. Tang, G. Grampp, Y. Liu, B.-X. Wang, F.-F. Tao, L.-J. Wang, X.-Z. Liang, H.-Q. Xiao, Y.-M. J. Shen, *J. Org. Chem.* **2015**, *80*, 2724–2732.

[27] L. Chu, C. Ohta, Z. Zuo, D. W. C. MacMillan, *J. Am. Chem. Soc.* **2014**, *136*, 10886-10889.

[28] a) C.-J. Wallentin, J. D. Nguyen, P. Finkbeiner, C. R. J. Stephenson, *J. Am. Chem. Soc*. **2012**, *134*, 8875–8884; b) J. D. Nguyen, E. M. D'Amato, J. M. R. Narayanam, C. R. J. Stephenson, *Nat. Chem*. **2012**, *4*, 854–859.

[29] An alternative mechanism involves an initial amine-mediated reduction of **5*** to its radical anion, followed by the reduction of alkyl halide **15** by **5**•⁻, with the regeneration of the ground state **5**. See Figure S87 and S88 in SI for details. For a selected mechanistic study see: R., Martinez-Haya, M. A. Miranda, M. L. Marin, *Eur. J. Org. Chem*. **2017**, *15*, 2164–2169.

[30] An indirect nucleophilic approach to the generation of benzylic radicals starting from benzyl halides has been recently reported. See: B. Schweitzer-Chaput, M. A. Horwitz, E. de Pedro Beato, P. Melchiorre, *Nat. Chem.* **2019**, *11*, 129-135.

[31] a) J. Bonin, C. Costentin, M. Mahet, J.-B. Mulon, M. Robert, *Phys. Chem. Chem. Phys*. **2009**, *11*, 10275-10280; b) G. Qiu, Y. Li, J. Wu, *Org. Chem. Front.* **2016**, *3*, 1011–1027.

[32] I. Ghosh, T. Ghosh, J. I. Bardagi, B. König, *Science* **2014**, **346**, 725–728.

[33] Mechanistically, the irreversibility of the process can explain the feasibility of this extremely reductive transformations. Slightly differences from the required oxidation potentials are possibly compensated by the irreversible formation of the aromatic radical and the iodide anion. For similar seminal examples see: a) I. Ghosh, R. S. Shaikh, B. König, *Angew. Chem. Int. Ed.* **2017**, *56*, 8544–8549; *Angew. Chem.* **2017**, 129, 8664–8669; b) M. Marchini, G. Bergamini, P. G. Cozzi, P. Ceroni, V. Balzani, *Angew. Chem. Int. Ed.* **2017**, *56*, 12820–12821; *Angew. Chem.* **2017**, 129, 12996–12997; c) I. Ghosh, J. I. Bardagi, B. König, *Angew. Chem. Int. Ed.* **2017**, 56, 12822–1282; *Angew. Chem*. **2017**,129, 12998–1300.

**Entry for the Table of Contents** (Please choose one layout)

Layout 2:

RESEARCH ARTICLE

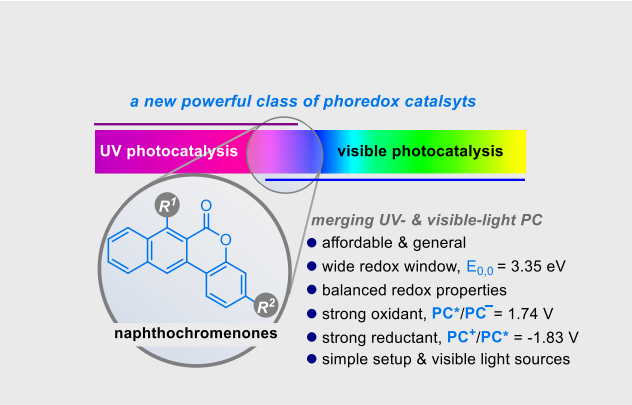


*Javier Mateos, Francesco Rigodanza, Alberto Vega-Peñaloza, Andrea Sartorel, Mirco Natali, Tommaso Bortolato, Giorgio Pelosi, Xavier Companyó, Marcella Bonchio, and Luca Dell'Amico**

***Page No. – Page No.***

**Naphthochromenones as Powerful Photoredox Catalysts. Synthesis, Structure-Property Relationship and Applications**